DynAMITe: a wafer scale sensor for biomedical applications



2011 JINST 6 C12064

(http://iopscience.iop.org/1748-0221/6/12/C12064)

PUBLISHED BY IOP PUBLISHING FOR SISSA

RECEIVED: *October 22, 2011*
ACCEPTED: *December 2, 2011*
PUBLISHED: *December 22, 2011*

THE 9th INTERNATIONAL CONFERENCE ON POSITION SENSITIVE DETECTORS,
12–16 SEPTEMBER 2011,
ABERYSTWYTH, U.K.

# DynAMITe: a wafer scale sensor for biomedical applications

**M. Esposito,[a,1] T. Anaxagoras,[b] A. Fant,[b] K. Wells,[a,c] A. Konstantinidis,[d] J.P.F. Osmond,[e] P.M. Evans,[e] R.D. Speller[d] and N.M. Allinson[b]**

[a] *Centre for Vision, Speech and Signal Processing, University of Surrey, Guildford GU2 7XH, U.K.*
[b] *School of Computer Science, University of Lincoln, Lincoln LN6 7TS, U.K.*
[c] *Department of Radiological Sciences, King Saud University, Riyadh 11451, Kingdom of Saudi Arabia*
[d] *Department of Medical Physics and Bioengineering, University College London, London WC1E 6BT, U.K.*
[e] *Joint Physics Department, Institute of Cancer Research and Royal Marsden NHS Trust, Sutton SM2 5PT, U.K.*

*E-mail:* m.esposito@surrey.ac.uk

ABSTRACT: In many biomedical imaging applications Flat Panel Imagers (FPIs) are currently the most common option. However, FPIs possess several key drawbacks such as large pixels, high noise, low frame rates, and excessive image artefacts. Recently Active Pixel Sensors (APS) have gained popularity overcoming such issues and are now scalable up to wafer size by appropriate reticule stitching. Detectors for biomedical imaging applications require high spatial resolution, low noise and high dynamic range. These figures of merit are related to pixel size and as the pixel size is fixed at the time of the design, spatial resolution, noise and dynamic range cannot be further optimized. The authors report on a new rad-hard monolithic APS, named DynAMITe (Dynamic range Adjustable for Medical Imaging Technology), developed by the UK MI-3 Plus consortium. This large area detector (12.8 cm$\times$12.8 cm) is based on the use of two different diode geometries within the same pixel array with different size pixels (50 $\mu$m and 100 $\mu$m). Hence the resulting device can possess two inherently different resolutions each with different noise and saturation performance. The small and the large pixel cameras can be reset at different voltages, resulting in different depletion widths. The larger depletion width for the small pixels allows the initial

[1] Corresponding author.


doi:10.1088/1748-0221/6/12/C12064

2011 JINST 6 C12064

generated photo-charge to be promptly collected, which ensures an intrinsically lower noise and higher spatial resolution. After these pixels reach near saturation, the larger pixels start collecting so offering a higher dynamic range whereas the higher noise floor is not important as at higher signal levels performance is governed by the Poisson noise of the incident radiation beam. The overall architecture and detailed characterization of DynAMITe will be presented in this paper.

KEYWORDS: Solid state detectors; Radiation-hard detectors; Pixelated detectors and associated VLSI electronics

2011 JINST 6 C12064

## Contents



2011 JINST 6 C12064

## 1 Introduction

Many biomedical applications like mammography [1], fluoroscopy [2], image-guided radiotherapy [3] and contact imaging in genomics and proteomics [4] require a large format sensor covering the entire imaging area and near real-time frame rates. The latter represents a great challenge for large area sensors [5]. Nowadays the most common detectors in this field are Flat Panel imagers (FPIs) which offer a reasonably large area, typically greater than 40 cm$\times$40 cm. Even so such detectors present severe drawbacks such as large pixels, high noise, low frame rate and excessive image artefacts. In the last two decades Active Pixel Sensors (APSs) have gained popularity because of a potential for overcoming such issues, allowing a high frame rate, due to a column parallel readout together with low power consumption and relatively low cost. Furthermore, in recent years, improvements in design and fabrication techniques have made available constructive processes for wafer scale imagers, which can now be seamlessly scaled from a few centimeters square up to the wafer size [1, 6]. A number of large area CMOS detectors are commercially available, though they suffer a relatively poor conversion gain and detection efficiency and a low frame rate. For example the Dalsa VLA CMOS APS [7] presents an active area of 49 mm $\times$ 98 mm with 96 $\mu$m pixel and is 3-side buttable reaching a larger area when tiled. It has a large dynamic range (85 dB) but a poor conversion gain of 0.21 $\mu$V/$e^-$. The RadIcon RedEye 1 [8] measures 98 mm by 49 mm and is 3-sides buttable. It has a relatively low read noise (150 $e^-$) but a relatively poor conversion gain (0.2 $\mu V/e^-$). A suitable detector for biomedical imaging applications needs to fulfill specific requirements in terms of spatial resolution, noise and dynamic range. An ideal detector for biomedical imaging applications should have high spatial resolution, low noise and high dynamic range. These performance levels are connected with the pixel size: a larger pixel leads to a lower spatial resolution, a higher noise and saturation level than a smaller one. Since the pixel size is fixed at

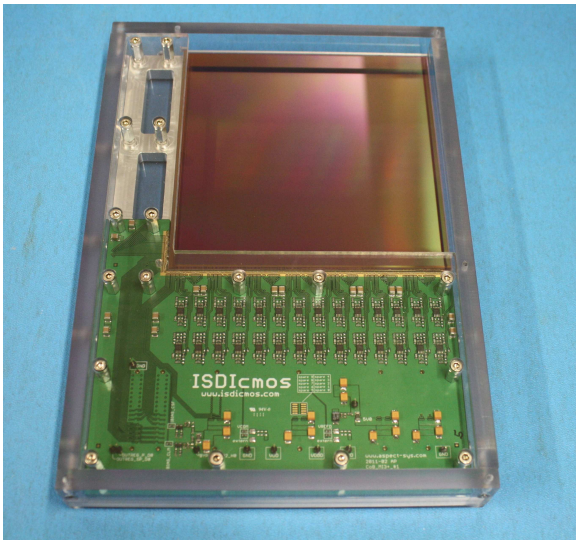


**Figure 1**. The DynAMITe detector in its first deployment.

the time of the design, spatial resolution, noise and dynamic range cannot be further optimized. In this paper the authors propose a novel wafer scale APS based on the use of two different diode geometries in the same pixel array and with different size active pixels. As the effective pixel size is no longer fixed, but two different pixel sizes are used for the whole detector matrix, this detector can deliver high spatial resolution, low noise and high dynamic range simultaneously.

## 2 Materials and methods

### 2.1 Detector

A new radiation hard monolithic APS has been developed by the Multidimensional Integrated Intelligent Imaging Plus (MI-3 Plus) consortium (RC-UK EP/G037671/1 programme). This APS, known as the Dynamic range Adjustable for Medical Imaging Technology or DynAMITe sensor (see figure 1), was constructed in a 0.18 $\mu$m CMOS process by using a reticule stitching technique [6] for a total active area of 12.8 cm $\times$ 12.8 cm. Since DynAMITe is two-side buttable, a larger active area can be achieved up to 25.6 cm $\times$ 25.6 cm which means it can deliver an imaging area highly comparable to flat panel array technology. The pixel array has been designed to realize two imagers in one by using different size light-converting elements meshed in the same pixel matrix. The detector consists of fine-pitch grid diodes, offering intrinsic low noise and high spatial resolution, superimposed on a set of a large-pitch grid diodes, offering a high dynamic range. Thus each cell of the DynAMITe matrix is fitted with multiple diodes: four diodes of small size (50 $\mu$m side), referred to as Sub-Pixels, and one diode of large size (100 $\mu$m side), referred to as Pixel. The whole matrix comprises 1260 $\times$1280 Pixels and 2520 $\times$ 2560 Sub-Pixels (see figure 2 (*left*)). Each light-converting element is designed in a standard 3-T architecture [9], allowing a reasonably high Fill Factor (70%) and Quantum Efficiency (QE) estimated as 45% for 523 nm light. The Sub-Pixel diodes and the Pixel diodes are reset at different voltages, resulting in the generation of different depletion widths. The higher voltage at which the Sub-Pixel diodes are reset allows the first gen-



2011 JINST 6 C12064

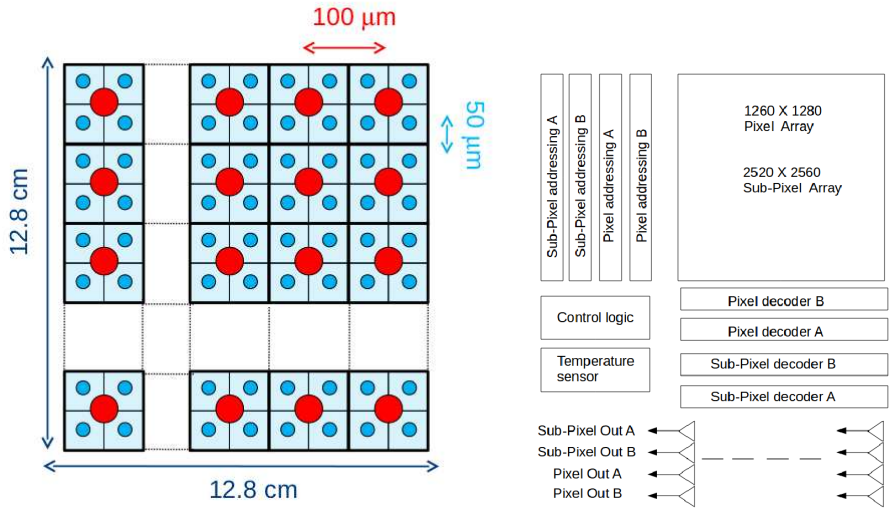


**Figure 2**. A schematic of the pixel array arrangement(*left*). Red circles represent the large size diodes placed at 100 $\mu$m pitch (Pixels). Cyan circles represent the small size diodes placed at 50 $\mu$m pitch (Sub-Pixels). A block diagram of the internal architecture of the DynAMITe detector (*left*).

erated photo-electrons to be rapidly collected by the Sub-Pixel diodes which ensures an intrinsic lower noise and a higher spatial resolution. Only after the Sub-Pixels reach near saturation, do the Pixel diodes start collecting significant amount of charge, so offering a higher dynamic range due to their larger collecting area compared to the Sub-Pixels. This process offsets the higher noise related to the Pixels diodes and does not significantly degrade the global performance. In fact, with a proper choice of the depletion voltages of both diode types, the large diodes collect only the charge exceeding the saturation level of the small diodes. Under this design the Pixels collect only high intensity signals, so that the higher noise, due to the larger diode size, is not important as at higher signal levels performance is governed by the inherent Poisson noise of the incident radiation flux. With these design choices the DynAMITe detector represents a new type of active image sensor capable of simultaneous low noise and high resolution, due to the Sub-Pixels, and a high dynamic range with a low noise due to the Pixels. A block diagram of the sensor is shown in figure 2 (*right*) where four independent read out circuits (addressing and decoders) are shown. In fact the readout, performed on a column parallel basis, is designed with two independent readout circuits for both small and large diodes matrices to perform dual readout addressing for each diode. This choice allows two parallel readout cycles for each matrix, leading to a significant increase in the frame rate: up to 30 fps for the Sub-Pixel array and 90 fps for the Pixel array. Further, different reset voltage can selectively choose the operating resolution of the detector leading to true pixel binning.

Both the Pixel and Sub-Pixel matrices can be read in combination, or separately with different exposure time in destructive or non destructive mode. Furthermore user-defined regions of Sub-Pixels can be read out selectively for dose sensing and on-line evaluation of the required exposure time. DynAMITe has also been designed according to radiation hardness requirements, using enclosed geometry layout (Enclosed Layout Transistor) [10].[1]

[1]The radiation hardness of this sensor has been evaluated by means of a test structure comprising this pixel architecture. The test sensor has been irradiated with 1.3 MeV photons showing no significant increasing in leakage current up to a radiation dose of 2 kGy.



2011 JINST 6 C12064

### 2.2 Optical performance evaluation

Accurate characterization of device performance is critical in scientific imaging, particularly for medical and biological imaging, where it is required to ensure device performance is suitable for the intended application. Device characterization in terms of parameters like conversion gain, noise, quantum efficiency and full well capacity are also needed for optimization of system performance. Mean-variance analysis is the gold standard for derivation of the conversion gain parameter for CCD and CMOS sensors [11, 12] and is used here as described below. Assuming a linear signal model, the total temporal variance $\sigma_S^2$ of the digital signal $S$ produced by $N$ interacting photons is given by

$$\sigma_S^2 = G^2\sigma_d^2 + \sigma_q^2 + G(\mu_S - \mu_{\text{dark}}) \tag{2.1}$$

where $G$ is the conversion gain expressed in $DN/e^-$, $\sigma_d^2$ is the signal variance due the normal-distributed noise in the amplifiers and readout circuits, $\sigma_q^2$ is the signal variance due to the uniform-distributed quantization noise, $\mu_S$ is the mean value of the signal $S$ at a given illumination corresponding to $N$ incident photons and $\mu_{\text{dark}}$ is the mean value of the signal corresponding to dark exposure. The square root of the sum of the first two terms is also referred to as read noise $\sigma_r$. Plotting $\sigma_S^2$ versus $\mu_S - \mu_{\text{dark}}$ yields a mean-variance graph. According to equation 2.1, the slope of the mean-variance graph provides the conversion gain $G$ whereas the square root of the intercept provides the read noise $\sigma_r$. The mean-variance curve data are generated by varying the light intensity of a uniformly irradiated $256 \times 256$ pixel region of the sensor from dark until saturation. The following parameters can be derived once the conversion gain has been calculated.

1. Linear range is the region over which the response of the sensor deviates from linearity by less than 5% in the mean-variance curve.

2. Full well capacity, determined using the product of the signal level at which the maximum variance occurs and the conversion gain: $FW = KS_{\text{max}}$

3. Dynamic range: $DR = 20log(FW/\sigma_r)$

4. Quantum efficiency $\eta$ estimated from the slope of the transfer function between sensor signal output and input in photons.

5. Integral non linearity, which is the difference between the data points and the linear regression fit to to the linearity graph computed as $INL = (S_{\text{max}} - S_{\text{min}})/ADC_{\text{fullscale}} \times 100$

In order to optically characterize the Sub-Pixel camera performance, DynAMITe was mounted on an optical test bench combined with an LED array producing illumination centred at 523 nm (bandwidth 35 nm) with a lens to achieve uniform illumination and a single neutral density filter. This setup followed the standard protocol for achieving flat field illumination provided by the Standard 1288 of European Machine Vision Association [13]. The sensor was exposed to green light varying the illumination level from 0 to 70 nW/cm$^2$. Multiple frames were acquired for each illumination value with an exposure time of 160 ms and averaged. Calculations were performed in a $256 \times 256$ pixel Region of Interest (ROI) in a single stitching block in order to avoid any stitching related fixed pattern noise.

2011 JINST 6 C12064

### 2.3 Non destructive readout

The dual readout circuits of both large and small diode matrices facilitate non destructive readout. The full frame of the entire pixel matrix (referred to as primary camera) can be readout at a given frame rate while an ROI (referred to as secondary camera) is simultaneously readout at a higher frame rate. One of the two readout chains is used for the primary camera whereas the other chain addresses the secondary camera. If the reset signal is disabled for the secondary camera, this camera is reset only via the reset signal for the primary camera allowing charge to be integrated in the ROI for an exposure time equal to the one at which the whole matrix is readout. This functionality was tested in order to evaluate the charge collection and noise performance. The DynAMITe sensor was exposed to a 523 nm LED with a brightness of 20 nW/cm$^2$. A $512 \times 2513$ pixel ROI was defined and readout at 26.3 fps, whereas the whole matrix was readout at 3.6 fps. For comparison a similar data set, with the same illumination conditions and exposure time, was acquired for the primary camera operating without the non destructive ROI. Mean signal and noise were analyzed for each of these conditions. Noise was calculated evaluating the standard deviation of the difference of two consecutive frames.

### 2.4 Charge collection test

The dual pixel geometry of the DynAMITe detector is based on the combined operation of different size diodes. Thus, the charge collection process for each diode type was tested as described below. The sensor was exposed to a uniform illumination field provided by an LED array at 523 nm with illumination level increasing from 0 to 350 nW/cm$^2$. The signal amplitude from both the Sub-Pixel and Pixel cameras operating synchronously with 190 ms integration time was measured. A further test was performed in order to evaluate any potential lack of charge collected in the Sub-Pixel camera due to the Pixel camera collecting at the same time. The sensor was exposed to a uniform illumination field with the illumination level increasing from 0 to 500 nW/cm$^2$ with 190 ms integration time. The output signal of the Sub-Pixel camera was measured when it was operated alone and also when operated synchronously with the Pixel camera.

## 3 Results

Figure 3 shows the mean-variance graph for the DynAMITe sensor. Signal variance per pixel is plotted versus the mean signal per pixel after dark subtraction. Using the integral slope of the linear region (65% dynamic range), the conversion gain $K$ was calculated as $50.0 \pm 0.2$ $e^-/DN$. Using this value of conversion gain a read noise $\sigma_r$ of $149.9 \pm 0.7$ $e^-$, a full well capacity $FW$ of $(2.8 \pm 0.2) \times 10^5$ $e^-$ and a dynamic range of 65 dB were obtained. The linearity curve of the detector is shown in figure 4. The signal per pixel (electrons) calculated using the conversion gain is plotted as function of the number of photons hitting the pixel. The slope of this curve yields a quantum efficiency, $\eta$, of 45%. The integral non linearity was estimated to be as low as 0.4%. Figures 5 and 6 shows the non destructive readout testing. The mean signal, figure 5, or the noise rms, figure 6, is represented as function of the time for the ROI of the secondary camera readout at 26.3 fps (black squares), for the full frame of the primary camera readout at 3.6 fps simultaneously with the secondary camera (red circles) and for the full frame of the primary camera readout at



2011 JINST 6 C12064

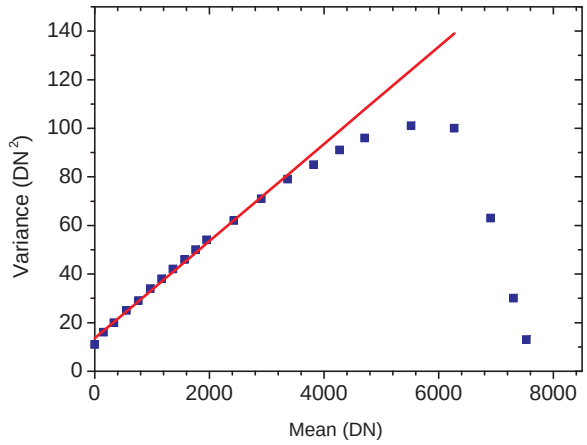


**Figure 3**. (Mean-variance graph: signal variance per pixel is plotted versus the mean signal per pixel after dark subtraction. A linear fit is also indicated.

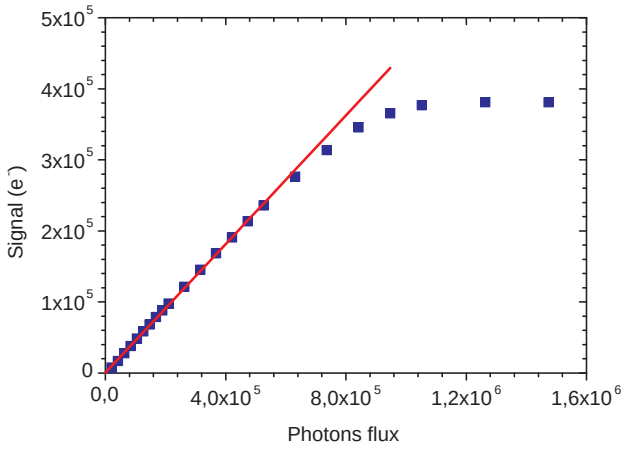


**Figure 4**. Linearity curve: signal per pixel in electrons calculated using the conversion gain is plotted as function of the number of photons hitting the pixel. A linear fit is also indicated.

3.6 fps alone (blue triangles). Figure 7 shows the sensor output versus illumination level for both Sub-Pixel and Pixel cameras. The Sub-Pixel camera collects with higher efficiency than the Pixel camera until the small diodes reach saturation. Sub-Pixels reach saturation at about 40 nW/cm$^2$ when Pixels are at the 14% of their dynamic range given 190 ms integration time. After this point Pixels collect all the high intensity signal with a linear behavior over the complete range investigated (0–350 nW/cm$^2$) and reach saturation at the end of this interval. The output signal for the Sub-Pixel camera is shown in figure 8 varying the illumination from 0 to 500 nW/cm$^2$. The signal of the small pixel camera is measured when the Sub-Pixels collect alone (i.e. Pixels are disabled) and in the case that Pixels and Sub-Pixels work synchronously. There is no appreciable difference in the Sub-Pixels output in the two different conditions.



2011 JINST 6 C12064

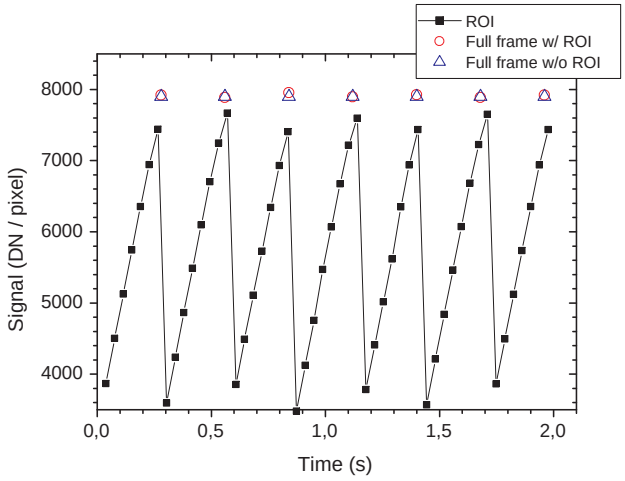


**Figure 5**. Non destructive readout testing. The mean signal from non destructive readout is represented as function of time for the ROI of the secondary camera. This is readout at 26.3 fps (black squares), which effectively produces a linearly increasing integration time. The full frame of the primary camera is readout at 3.6 fps simultaneously with the secondary camera (red circles). The full frame of the primary camera alone is readout at 3.6 fps (blue triangles).

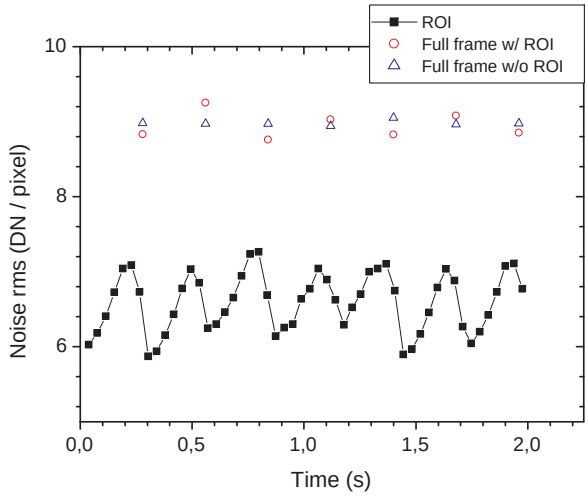


**Figure 6**. Non destructive readout testing. Noise level for the Sub-Pixel camera (black squares) and for the Pixel camera (red circles) operating synchronously varying the illumination level.

## 4 Discussion

The optical performance of the DynAMITe CMOS APS was quantitatively evaluated and a selection of the working modalities were tested. The optical performance of the Sub-Pixel camera of DynAMITe detector is next compared with several of state-of-the-art large area CMOS detector both from commercial companies and academia: the RadIcon RedEye 1 CMOS APS [8]; the



2011 JINST 6 C12064

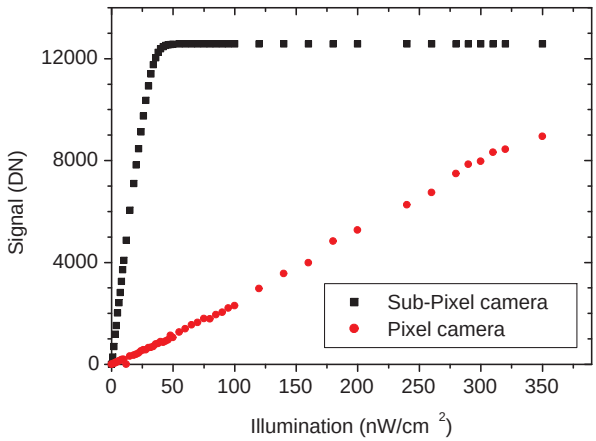


**Figure 7**. Non destructive readout testing. The noise rms from non destructive readout (*right*) is represented as function of time for the ROI of the secondary camera readout at 26.3 fps (black squares). The full frame of the primary camera is readout at 3.6 fps simultaneously with the secondary camera (red circles). The full frame of the primary camera alone is readout at 3.6 fps (blue triangles).

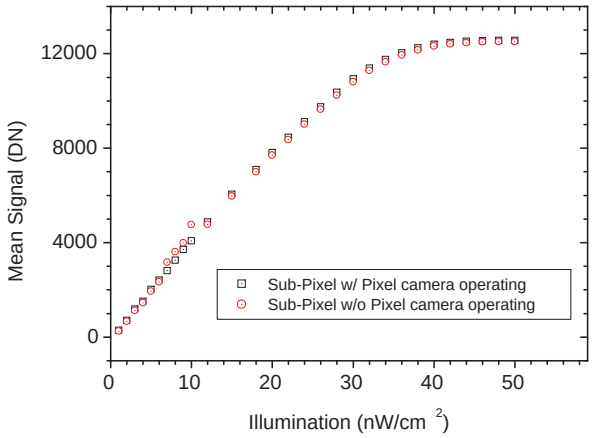


**Figure 8**. Output signal for the Sub-Pixel camera operating alone (red circles) or synchronously with Pixel camera operating synchronously (black squares) varying the illumination level.

Hamamatsu C97732 DK-11 CMOS Passive Pixel Sensor (PPS) [14]; the Dalsa CMOS APS [15]; the Very Large Area (VLA) CMOS sensor from Dalsa [7]; the CMOS APS developed by Micron Technology and Univeristy of Southern California [16]; the MI3 Large Area Sensor (LAS) CMOS APS [1, 17]. The comparisons are shown in tables 1 and 2. The DynAMITe detector offers the largest area ($12.8 \times 12.8$ cm$^2$) for the single sensor, further expansible up to 25.6 cm $\times$25.6 by means of the two-side butt-ability. The maximum frame rate for the full frame readout is the highest among the competitors. The Sub-Pixel camera frame rate is between 3 and 30 times greater than the state-of-the-art commercial devices such as (RadIcon RedEye 1, Hamamatsu C97732 DK-11,



2011 JINST 6 C12064

**Table 1**. Summary of the design specifications for CMOS large area detectors.

| | Area ($cm^2$) | Side buttable | Pixel size ($\mu$m) | No. of pixel | Frame rate (fps) |
|---|---|---|---|---|---|
| RedEye1 [8] (RadIcon) | 2.46×4.92 | 3 | 48 | 512×1024 | 4.5 |
| C97732 DK-11 [14] (Hamamatsu) | 12×12 | — | 50 | 2400×2400 | 1 |
| CMPS APS [15] (Dalsa) | 7.73×14.5 | 3 | 33.55 | 2304×4320 | 8.7 |
| VLA CMOS [7] (Dalsa) | 4.9×9.8 | 3 | 96 | 512×1024 | 1.3 |
| CMOS APS [16] (Micron Technology) | 7.37×7.75 | — | 18 | 4096×4114 | 1.25 |
| LAS [1, 17] (MI3) | 5.6×5.6 | — | 40 | 1350×1350 | 20 |
| DynAMITe [This work] (MI3+) | 12.8×12.8 | 2 | 50 | 2520×2560 | 30 |

Dalsa and Micron Technology APSs) and is 1.5 times greater than the frame rate for LAS with over three times as many pixels. The comparative data for noise floor, conversion gain, dynamic range and quantum efficiency indicate that the DynAMITe system is the most sensitive and efficient among the devices involved in this comparison. The conversion gain (50.0 $e^-$/DN, 2.1 $\mu$V/DN) of DynAMITe is comparable with the highest among the conversion gain values for the systems included in table 2 (Dalsa and Micron Technology CMOS APSs). The quantum efficiency at green light, $\eta$, measured for the DynAMITe imager (45% or 64% including the fill factor) is the highest in table 2. The noise floor is in the middle of the range of the noise floor values for the APS (RadIcon RedEye 1, LAS, Dalsa CMOS APS, Dalsa VLA CMOS, Micron Technology CMOS APS), whereas this value is expected to be higher for the PPS [18] (Hamamatsu C97732 DK-11). The dynamic range of the DynAMITe Sub-Pixel camera (65 dB or 69 dB when Correlated Double Sampling is applied) is higher than that of LAS but lower than that offered by the other detectors. This limitation can be addressed when both cameras of the DynAMITe sensor operate together. In fact combining Sub-Pixel and Pixel performance realizes a higher dynamic range due to a higher saturation level related to the larger size diode - estimated 3 times larger than the Sub-Pixel one, of the Pixel camera as shown if figure 7.

The non destructive read out architecture was tested evaluating signal and noise in both primary and secondary cameras and compared with the performance of the primary camera operating alone. The signal for each of the test condition proposed follows the integration pattern defined for the non destructive readout. The signal and noise for the primary camera operating with and without the secondary camera are comparable. Thus when operating simultaneously, both readout schemes can operate independently without compromising sensor performance. The noise measured in the ROI of the secondary camera represents 35% lower noise compared with the primary



2011 JINST 6 C12064

**Table 2**. Performance comparison for large area CMOS detector.

| | Noise floor ($e^-$) | Conversion gain | Dynamic range (dB) | $\eta$ @520 nm (%) |
|---|---|---|---|---|
| RedEye 1 [8] (RadIcon) | 150 (@1 fps) | 0.5 $\mu V/e^-$ | 84 | — |
| CMOS APS [15] (Dalsa) | 175 | 2.45 $\mu$V/e$^-$ | 71.4 | — |
| VLA CMOS [7] (Dalsa) | 250 | 0.21 $\mu$V/e$^-$ | 85 | (45)[a] |
| C97732 DK-11 [14] (Hamamatsu) | 1250 | — | 74 | — |
| CMOS APS [16] (Micron Technology) | 240 | 2.27 $\mu$V/e$^-$ | 75 | (46)[a,b] |
| LAS [1, 17] (MI3) | 50 | 4.6 e$^-$/DN | 63 | 18 |
| DynAMITe [This work] (MI3+) | 150 (97.5)[c] | 50 e$^-$/DN (2.1 $\mu V/e^-$) | 65 (69)[c] | 45 (64)[a] |

[a] Quantum efficiency including fill factor [b] Extrapolated [c] CDS applied

camera (both with and without ROI selection). This is because of Correlated Double Sampling (CDS) [18, 19] resulting from image subtraction for the secondary camera. As CDS suppresses offset Fixed Pattern Noise (FPN) and reset noise, the noise level measured with non destructive readout can give an estimation of the influence of the reset noise with respect to the global noise of the sensor measured in equation 2.1.

## 5 Conclusions

The DynAMITe detector has been presented as a novel, radiation hard, large area APS imaging sensor capable of two inherently different resolutions each with different noise and saturation performance in the same pixel array. Optical performance has been evaluated for the Sub-Pixel camera with 50 $\mu$m pixels. This exhibits a conversion gain of 50.0 $e^-/DN$ and a readout noise of 150 $e^-$. The quantum efficiency at 523 nm was measured as 45%, which is reasonably high given a fill factor of 70%. The measured performance for the 50 $\mu$m camera exceeds the performance of state-of-the-art large area CMOS detectors [1, 8, 14, 17]. Operating simultaneously both Pixel and Sub-Pixel cameras can be expected to provide a significant step forward to the overall performance of APS devices in terms of dynamic range, resolution and frame rate. The DynAMITe design has great potential for use in a variety of biomedical imaging applications fulfilling the requirement of large imaging area with high dynamic range and frame rate. The authors are currently developing demonstrator applications in radiotherapy portal imaging, X-ray breast mammography, X-ray diffraction studies for breast cancer diagnosis and molecular sequencing methods for the life sciences.



2011 JINST 6 C12064

## Acknowledgments

This work was supported by the EPSRC Multidimensional Integrated Intelligent Imaging Plus (MI-3 Plus) programme (EP/G037671/1).

## References

[1] S.E. Bohndiek et al., *Characterization and testing of LAS: a prototype 'Large Area Sensor' with performance characteristics suitable for medical imaging applications*, *IEEE Trans. Nucl. Sci.* **56** (2009) 2938.

[2] A.R. Cowen et al., *Solid-state, flat-panel, digital radiography detectors and their physical imaging characteristics*, *Clin. Radiol.* **63** (2008) 487.

[3] J. Osmond et al., *An investigation into the use of CMOS active pixel technology into image-guided radiotherapy*, *Phys. Med. Biol.* **53** (2008) 3159.

[4] M. Gersbach et al., *A room temperature CMOS single photon sensor for chemiluminescence detection*, in the proceedings of the *Internation Conference on Miniaturized Systems for Chemistry and Life Science (MicroTas)*, November 5–9, Tokyo, Japan (2006).

[5] R. Turchetta et al., *Large area CMOS image sensors*, 2011 *JINST* **6** C01099.

[6] D. Scheffer et al., *Wafer scale active pixels CMOS image sensor for generic X-ray radiology*, *Proc. SPIE* **6510** (2007) 65100O.

[7] M. Farrier et al., *Very large area CMOS active-pixel sensor for digital radiography*, *IEEE Trans. Electron. Dev.* **56** (2009) 2623.

[8] RadIcon Imaging Corporation, *RadEye1*, http://www.rad-icon.com/products-radeye.php (2011).

[9] E.R. Fossum et al., *CMOS image sensors: electronic camera-on-a-chip*, *IEEE Trans. Electron. Dev.* **44** (1997) 1689.

[10] F. Faccio et al., *Total dose and single event effects (SEE) in a* $0.25\,\mu m$ *CMOS technology*, in the proceedings of the $4^{th}$ *Workshop on Electronics for LHC Experiments*, September 21–25, Rome, Italy (1998).

[11] B. Stark et al., *Method for determining the electron number in charge-coupled measurement devices*, *Opt. Eng.* **31** (1992) 852.

[12] B.P. Beecken et al., *Determination of the conversion gain and the accuracy of its measurements for detector elements and arrays*, *Appl. Opt.* **35** (1996) 3471.

[13] European Machine Vision Association, *Standard for characterization and presentation of specification data for image sensors and cameras*, EMVA Standard 1288 (2005).

[14] Hamamatsu, *X-ray flat panel imagers for radiology*, http://sales.hamamatsu.com/en/products/solid-state-division/x-ray-flat-panel-sensor/for-radiology/part-c9732dk-11.php (2011).

[15] L. Korthout et al. *A wafer-scale CMOS APS imager for medical X-ray applications*, in the proceedings of the 2009 *International Image Sensor Workshop* June 22–28, Bergne, Norway (2009), paper 70.

[16] S.U. Ay and E.R. Fossum, *A* $76 \times 77\,mm^2$, *16.85 million pixel CMOS APS image sensor*, in *IEEE Symposium on VLSI Circuit, Digest of Technical Papers* (2006) 19.



2011 JINST 6 C12064

[17] A. Konstantinidis et al., *Optical characterisation of a CMOS active pixel sensor using periodic noise reduction techniques*, *Nucl. Instrum. Meth.* **A 620** (2010) 549.

[18] A. El Gamal et al., *CMOS image sensors*, *IEEE Circ. Dev.* **21** (2005) 6.

[19] P.F.I. Scott et al., *A high dynamic range camera with a non destructive readout complementary metal oxide semiconductor sensor*, *Meas. Sci. Technol.* **20** (2009) 104004.

2011 JINST 6 C12064